2014 IEEE International Conference on Robotics & Automation (ICRA)
Hong Kong Convention and Exhibition Center
May 31 - June 7, 2014. Hong Kong, China

Impedance Control of VToL UAVs with a Momentum-based External Generalized Forces Estimator

Fabio Ruggiero[1], Jonathan Cacace[1], Hamid Sadeghian[2], and Vincenzo Lippiello[1]

Abstract— **An estimator of external generalized forces (force plus moments) acting on aerial platforms, and based on the momentum of the mechanical system, is proposed for the control of VToL UAVs together with a hierarchical architecture separating the translational and rotational dynamics of the vehicle. The closed-loop system equations are shaped as mechanical impedances, programmable through the controller gains, and forced by the residuals given by the estimation error. This arrangement allows the VToL UAVs to perform hovering and tracking tasks without a precise knowledge of the vehicle dynamics and in presence of external disturbances and unmodeled aerodynamic effects. Experiments are presented to evaluate the performance of the proposed control design.**

I. Introduction

The use of Vertical Take-Off and Landing (VToL) Unmanned Aerial Vehicles (UAVs) is growing day by day as well as the interest of the robotic research community towards such systems. These platforms are extensively employed in "passive" applications like inspection [1], [2], surveillance, monitoring, remote sensing, and many others. More recently, the UAVs have been also employed in "active" tasks like grasping [3] and manipulation [4], [5], [6], [7].

In both the aforementioned cases, high performance is requested to control such aerial vehicles. A number of different approaches tackle the issues related to the stabilization and tracking of desired trajectories with the use of UAVs. Namely, backstepping [8], optical flow [9], vision [10], port-Hamiltonian [11], and several others. However, a hierarchical architecture [12], [13] is often taken into account since it is possible to highlight a time-scale separation between the linear (slow time-scale) and rotational (fast time-scale) dynamics of the aerial vehicle. Several of the above mentioned controllers implement an integral action to resist against external disturbances, e.g., wind, unmodeled aerodynamic effects, and so on. Recently, adaptive controls have been employed to counteract such external disturbances [14], [15], [16]. Finally, impedance control represents an effective approach to control actively the compliance of a robotic system. However, it is usually necessary to have an estimation of external interaction on the system. To this end, suitable observers have been proposed to estimate collision forces [17], [18].

In this paper, starting from the hierarchical architecture presented in [13], a controller ensuring a closed-loop impedance behaviour for both the translational and rotational parts of a VToL UAV is proposed. In detail, the linear and angular tracking errors act like mass-spring-damper mechanical systems, in which the spring and damper coefficients are imposed through the choice of PD based controllers gains. The collision identification technique (based on the system momentum) proposed in [17] has been suitably modified and adapted as an estimator of external generalized forces (forces plus moments) acting on the aerial vehicle. The residual error between the estimated external generalized forces and the real ones is the forcing action of the closed-loop mass-spring-damper systems. Several experiments have been performed to prove the performance of the proposed controller design.

One among the benefits of the proposed controller is the small number of parameters that have to be tuned: no integral action is present and the gains of the estimator can be chosen on the basis of closed-loop impedance behaviour. Moreover, as it will be explained in the next sections, the estimator perfectly recovers constant external disturbances, while it recovers the time-varying ones on the basis of the chosen closed-loop bandwidth of the impedance. As a drawback, in case the frequency of the controller is too slow with respect to the one of the external disturbances, the compensation of the external generalized forces can worsen the performance of the control design. Nevertheless, as underlined in [19], even the use of adaptive or integral control actions may add a further disturbance instead of reduce it.

The outline of the paper is as follows. In the next section the modeling of the quadrotor is briefly revised. Section III introduces the momentum-based estimator of external generalized forces, while Section IV describes the proposed controller. A sketch of the stability proof is given in Section V, while Section VI provides experimental results. Conclusion and future work are finally illustrated.

II. Modeling

Without loss of generality, the remainder of the paper takes into account one of the most popular configuration of VToL UAVs, i.e., a *quadrotor*, which is a platform equipped with four propellers aligned in the same direction and placed either in cross or in plus configuration. The quadrotor is

The research leading to these results has been supported by the ARCAS and SHERPA collaborative projects, which both have received funding from the European Community Seventh Framework Programme (FP7/2007-2013) under grant agreements ICT-287617 and ICT-600958, respectively. The authors are solely responsible for its content. It does not represent the opinion of the European Community and the Community is not responsible for any use that might be made of the information contained therein.

[1]Fabio Ruggiero, Jonathan Cacace and Vincenzo Lippiello are with the PRISMA Lab, Dipartimento di Ingegneria Elettrica e Tecnologie dell'Informazione, Università degli Studi di Napoli Federico II, via Claudio 21, 80125, Naples, Italy.

[2]Hamid Sadeghian is with the Department of Biomedical Engineering, Faculty of Engineering, University of Isfahan, Isfahan 8174673441, Iran.

Corresponding author's email fabio.ruggiero@unina.it

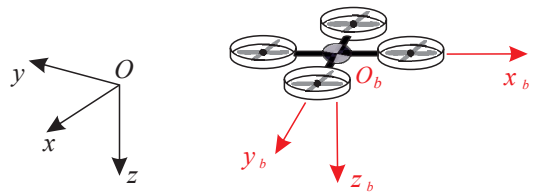

Fig. 1. Quadrotor and related frames.

an underactuated mechanical system having six degrees of freedom but only four control inputs.

Let $\Sigma_i, O-x,y,z$ and $\Sigma_b, O_b-x_b,y_b,z_b$ be the world-fixed inertia reference frame and the body-fixed frame placed at the UAV center of mass, respectively (see Fig. 1). The absolute position of the UAV with respect to Σ_i is denoted by $\boldsymbol{p}_b = \begin{bmatrix} x & y & z \end{bmatrix}^{\mathrm{T}}$, while the attitude is denoted by the rotation matrix $\boldsymbol{R}_b(\boldsymbol{\eta}_b) \in \mathrm{SO}(3)$, i.e., the rotation of Σ_b with respect to Σ_i, which is also described through a minimal representation by the roll-pitch-yaw Euler angles $\boldsymbol{\eta}_b = \begin{bmatrix} \phi & \theta & \psi \end{bmatrix}^{\mathrm{T}}$. Let $\dot{\boldsymbol{p}}_b$ and $\boldsymbol{\omega}_b$ denote the linear and angular velocities, respectively, with respect to Σ_i, while $\dot{\boldsymbol{p}}_b^b$ and $\boldsymbol{\omega}_b^b$ are expressed with respect to Σ_b. Denoting with $\dot{\boldsymbol{\eta}}_b$ the time derivative of $\boldsymbol{\eta}_b$, the following equations hold [20]

$$\dot{\boldsymbol{p}}_b = \boldsymbol{R}_b(\boldsymbol{\eta}_b)\dot{\boldsymbol{p}}_b^b, \tag{1a}$$
$$\boldsymbol{\omega}_b = \boldsymbol{T}_b(\boldsymbol{\eta}_b)\dot{\boldsymbol{\eta}}_b, \tag{1b}$$
$$\boldsymbol{\omega}_b^b = \boldsymbol{R}_b(\boldsymbol{\eta}_b)^{\mathrm{T}}\boldsymbol{\omega}_b = \boldsymbol{R}_b(\boldsymbol{\eta}_b)^{\mathrm{T}}\boldsymbol{T}_b(\boldsymbol{\eta}_b)\dot{\boldsymbol{\eta}}_b = \boldsymbol{Q}(\boldsymbol{\eta}_b)\dot{\boldsymbol{\eta}}_b, \tag{1c}$$

where $\boldsymbol{T}_b(\boldsymbol{\eta}_b)$ is the (3×3) transformation matrix between the time derivative of $\boldsymbol{\eta}_b$ and the correspondent $\boldsymbol{\omega}_b$, while $\boldsymbol{Q}(\boldsymbol{\eta}_b) = \boldsymbol{R}_b(\boldsymbol{\eta}_b)^{\mathrm{T}}\boldsymbol{T}_b(\boldsymbol{\eta}_b)$ maps the time derivative of $\boldsymbol{\eta}_b$ into the UAV angular velocity expressed with respect to Σ_b. The detailed expressions of $\boldsymbol{R}_b(\boldsymbol{\eta}_b)$ and $\boldsymbol{Q}(\boldsymbol{\eta}_b)$ are given in [13], [20] and they present a singularity at $\theta = \pm\pi/2$.

The dynamic equations of the UAV can be obtained by using the Newton-Euler formulation [13]

$$m\ddot{\boldsymbol{p}}_b^b + m\boldsymbol{S}(\boldsymbol{\omega}_b^b)\dot{\boldsymbol{p}}_b^b - m\boldsymbol{R}_b(\boldsymbol{\eta}_b)^{\mathrm{T}}\boldsymbol{g} = \boldsymbol{f}_b^b, \tag{2a}$$
$$\boldsymbol{I}_b\dot{\boldsymbol{\omega}}_b^b + \boldsymbol{S}(\boldsymbol{\omega}_b^b)\boldsymbol{I}_b\boldsymbol{\omega}_b^b = \boldsymbol{\tau}_b^b, \tag{2b}$$

where $\ddot{\boldsymbol{p}}_b^b$ is the absolute linear acceleration of the UAV expressed with respect to Σ_b, m is the mass of the vehicle, $\boldsymbol{I}_b$ is the (3×3) constant inertia matrix of the UAV expressed with respect to Σ_b, $\dot{\boldsymbol{\omega}}_b^b$ is the angular acceleration of the UAV expressed with respect to Σ_b, $\boldsymbol{S}(\cdot)$ denotes the skew-symmetric matrix operator [20], $\boldsymbol{g}$ is the (3×1) gravity vector $\boldsymbol{g} = \begin{bmatrix} 0 & 0 & g \end{bmatrix}^{\mathrm{T}}$, with $g = 9.81\mathrm{m/s}^2$, and $\boldsymbol{f}_b^b$ and $\boldsymbol{\tau}_b^b$ are the (3×1) force and torque input vectors, respectively, expressed with respect to Σ_b.

Folding (1) and the relative time derivatives into (2) yields the following dynamic model

$$m\ddot{\boldsymbol{p}}_b - m\boldsymbol{g} = \boldsymbol{R}_b(\boldsymbol{\eta}_b)\boldsymbol{f}_b^b, \tag{3a}$$
$$\boldsymbol{M}(\boldsymbol{\eta}_b)\ddot{\boldsymbol{\eta}}_b + \boldsymbol{C}(\boldsymbol{\eta}_b,\dot{\boldsymbol{\eta}}_b)\dot{\boldsymbol{\eta}}_b = \boldsymbol{Q}(\boldsymbol{\eta}_b)^{\mathrm{T}}\boldsymbol{\tau}_b^b, \tag{3b}$$

where $\boldsymbol{M}(\boldsymbol{\eta}_b) = \boldsymbol{Q}(\boldsymbol{\eta}_b)^{\mathrm{T}}\boldsymbol{I}_b\boldsymbol{Q}(\boldsymbol{\eta}_b)$ is the (3×3) positive definite inertia matrix (provided that $\theta \neq \pm\pi/2$), and $\boldsymbol{C}(\boldsymbol{\eta}_b,\dot{\boldsymbol{\eta}}_b) = \boldsymbol{Q}^{\mathrm{T}}\boldsymbol{S}(\boldsymbol{Q}\dot{\boldsymbol{\eta}}_b)\boldsymbol{I}_b\boldsymbol{Q} + \boldsymbol{Q}^{\mathrm{T}}\boldsymbol{I}_b\dot{\boldsymbol{Q}}$ is the (3×3) Coriolis matrix, in which the dependencies have been dropped and $\dot{\boldsymbol{Q}}(\boldsymbol{\eta}_b)$ represents the time derivative of $\boldsymbol{Q}(\boldsymbol{\eta}_b)$.

On the basis of the particular configuration of the considered VToL UAV, the expressions of the input forces, $\boldsymbol{f}_b^b$, and torques, $\boldsymbol{\tau}_b^b$, are different. Considering a quadrotor, this can be characterized by $\boldsymbol{\tau}_b^b = \begin{bmatrix} \tau_\phi & \tau_\theta & \tau_\psi \end{bmatrix}^{\mathrm{T}}$ and $\boldsymbol{f}_b^b = \begin{bmatrix} 0 & 0 & u \end{bmatrix}^{\mathrm{T}}$, where u denotes the total thrust perpendicular to the propellers rotation plane. The relationship between the thrust, the control torques and the forces f_i, with $i = 1,\dots,4$, generated by each of the four propellers is [21]

$$u = \sum_{i=1}^{4} f_i, \tag{4a}$$
$$\tau_\phi = l(f_2 - f_4), \tag{4b}$$
$$\tau_\theta = l(f_3 - f_1), \tag{4c}$$
$$\tau_\psi = cf_1 - cf_2 + cf_3 - cf_4, \tag{4d}$$

where l is the distance from the propollers to the center of mass of the quadrotor and $c > 0$ is the drag factor. Many aerodynamic effects are neglected through this representation, which is instead considered a good approximation in case of hovering or low-speed motion [13].

External forces, $\boldsymbol{f}_{ext}$, and moments, $\boldsymbol{\tau}_{ext}$, might act on the VToL UAVs during the execution of a task. Such external generalized forces may represent unmodeled aerodynamic effects, imbalances caused by batteries and/or on-board sensors, motion of a robotic arm placed for aerial manipulation actions, interactions with the environment, wind and so on. Hence, for control design purposes, the following dynamic model is considered

$$m\ddot{\boldsymbol{p}}_b - m\boldsymbol{g} = -u\boldsymbol{R}_b(\boldsymbol{\eta}_b)\boldsymbol{e}_3 + \boldsymbol{f}_{ext}, \tag{5a}$$
$$\boldsymbol{M}(\boldsymbol{\eta}_b)\ddot{\boldsymbol{\eta}}_b + \boldsymbol{C}(\boldsymbol{\eta}_b,\dot{\boldsymbol{\eta}}_b)\dot{\boldsymbol{\eta}}_b = \boldsymbol{Q}(\boldsymbol{\eta}_b)^{\mathrm{T}}\boldsymbol{\tau}_b^b + \boldsymbol{\tau}_{ext}, \tag{5b}$$

where $\boldsymbol{e}_3 = \begin{bmatrix} 0 & 0 & 1 \end{bmatrix}^{\mathrm{T}}$ and both $\boldsymbol{f}_{ext}$ and $\boldsymbol{\tau}_{ext}$ are (3×1) vectors.

III. Momentum-based External Generalized Forces Estimator

Along the lines of the approach described in [17], the (6×1) generalized momentum vector of the system (5) is defined as

$$\boldsymbol{q} = \begin{bmatrix} m\boldsymbol{I}_3 & \boldsymbol{O}_3 \\ \boldsymbol{O}_3 & \boldsymbol{M}(\boldsymbol{\eta}_b) \end{bmatrix} \begin{bmatrix} \dot{\boldsymbol{p}}_b \\ \dot{\boldsymbol{\eta}}_b \end{bmatrix}, \tag{6}$$

where $\boldsymbol{I}_n$ and $\boldsymbol{O}_n$ are $(n\times n)$ identity and zero matrices, respectively. From the properties of mechanical systems [20], it is possible to prove that

$$\dot{\boldsymbol{M}}(\boldsymbol{\eta}_b,\dot{\boldsymbol{\eta}}_b) = \boldsymbol{C}(\boldsymbol{\eta}_b,\dot{\boldsymbol{\eta}}_b) + \boldsymbol{C}(\boldsymbol{\eta}_b,\dot{\boldsymbol{\eta}}_b)^{\mathrm{T}}. \tag{7}$$

Using (5) and (7), the time derivative of the generalized momentum vector (6) is

$$\dot{\boldsymbol{q}} = \begin{bmatrix} -u\boldsymbol{R}_b(\boldsymbol{\eta}_b)\boldsymbol{e}_3 + \boldsymbol{f}_{ext} + m\boldsymbol{g} \\ \boldsymbol{Q}(\boldsymbol{\eta}_b)^{\mathrm{T}}\boldsymbol{\tau}_b^b + \boldsymbol{\tau}_{ext} + \boldsymbol{C}(\boldsymbol{\eta}_b,\dot{\boldsymbol{\eta}}_b)^{\mathrm{T}}\dot{\boldsymbol{\eta}}_b \end{bmatrix}. \tag{8}$$

The purpose of the proposed estimator is to achieve, in the Laplace domain, a linear relationship between the dynamics

of the estimated external generalized forces and the real ones. Hence, the following relationship can be written

$$\begin{bmatrix}\widehat{\boldsymbol{f}}_{ext}(s)\\ \widehat{\boldsymbol{\tau}}_{ext}(s)\end{bmatrix} = \boldsymbol{G}(s)\begin{bmatrix}\boldsymbol{f}_{ext}(s)\\ \boldsymbol{\tau}_{ext}(s)\end{bmatrix}, \tag{9}$$

where $\widehat{\boldsymbol{f}}_{ext}$ and $\widehat{\boldsymbol{\tau}}_{ext}$ are the (3×1) vectors of estimated external forces and moments, respectively, while $\boldsymbol{G}(s)$ is a (6×6) diagonal matrix of transfer functions in which the ith element, with $i=1,\dots,6$, has the following expression

$$G_i(s) = \frac{\omega_{n,i}^2}{s^2+2\zeta_i\omega_{n,1}s+\omega_{n,i}^2}, \tag{10}$$

with $w_{n,i}$ and ζ_i the desired natural frequency and damping factor of the system, respectively.

In order to get (10) component-wise in (9), the external generalized forces (in the time domain) has to be estimated as follows

$$\begin{bmatrix}\widehat{\boldsymbol{f}}_{ext}\\ \widehat{\boldsymbol{\tau}}_{ext}\end{bmatrix} = \boldsymbol{r}(t) = \boldsymbol{K}_1\left(\int_o^t -\boldsymbol{r}(t) + \boldsymbol{K}_2\Bigg(\boldsymbol{q}(t) - \int_0^t\left(\begin{bmatrix}-u\boldsymbol{R}_b(\boldsymbol{\eta}_b)\boldsymbol{e}_3+m\boldsymbol{g}\\ \boldsymbol{Q}(\boldsymbol{\eta}_b)^{\mathrm{T}}\boldsymbol{\tau}_b^b+\boldsymbol{C}(\boldsymbol{\eta}_b,\dot{\boldsymbol{\eta}}_b)^{\mathrm{T}}\dot{\boldsymbol{\eta}}_b\end{bmatrix}+\boldsymbol{r}(t)\right)ds\Bigg)ds\right), \tag{11}$$

where it is assumed that $\boldsymbol{q}(0)=\boldsymbol{r}(0)=\dot{\boldsymbol{r}}(0)=0$, while $\boldsymbol{K}_1=\mathrm{diag}\{\boldsymbol{K}_{1,1},\boldsymbol{K}_{1,2}\}$ and $\boldsymbol{K}_2=\mathrm{diag}\{\boldsymbol{K}_{2,1}\boldsymbol{K}_{2,2}\}$ are (6×6) positive definite diagonal matrices, in which $\boldsymbol{K}_{i,j}$, $i,j=\{1,2\}$, is a (3×3) positive definite diagonal matrix. Considering (5) and (8), the dynamics of (11) is

$$\ddot{\boldsymbol{r}}+\boldsymbol{K}_1\dot{\boldsymbol{r}}+\boldsymbol{K}_1\boldsymbol{K}_2\boldsymbol{r} = \boldsymbol{K}_1\boldsymbol{K}_2\begin{bmatrix}\boldsymbol{f}_{ext}\\ \boldsymbol{\tau}_{ext}\end{bmatrix}, \tag{12}$$

that in Laplace domain is equivalent to (10).

The natural frequencies and the damping factors in (10) can be chosen on the basis of the bandwidth of the closed-loop equations as explained in the next section. Once they have been designed, the components of the matrices $\boldsymbol{K}_1$ and $\boldsymbol{K}_2$ in (11) can be retrieved as follows

$$k_{1,i}k_{2,i} = \omega_{n,i}^2, \tag{13a}$$

$$k_{1,i} = 2\zeta_i\omega_{n,i}, \tag{13b}$$

where $i=1,\dots,6$, and $k_{1,i}$ and $k_{2,i}$ are the ith element of $\boldsymbol{K}_1$ and $\boldsymbol{K}_2$, respectively. In ideal case, notice that

$$\begin{matrix}\zeta_i\to 1\\ \omega_{n,i}\to\infty\end{matrix} \Longrightarrow \boldsymbol{r}(t) = \begin{bmatrix}\widehat{\boldsymbol{f}}_{ext}\\ \widehat{\boldsymbol{\tau}}_{ext}\end{bmatrix} \approx \begin{bmatrix}\boldsymbol{f}_{ext}\\ \boldsymbol{\tau}_{ext}\end{bmatrix},$$

with $i=1,\dots,6$, which means that the gains should be taken as large as possible in the practice. However, they have to take also into account the limitation given by the digital implementation of the controller. Hence, a good compromise has to be reached.

The quantities required to estimate the external generalized forces are the UAV attitude $\boldsymbol{\eta}_b$ and the related time derivative $\dot{\boldsymbol{\eta}}_b$, the vehicle linear velocity $\dot{\boldsymbol{p}}_b$, the commanded input torque $\boldsymbol{\tau}_b^b$ and thrust u, the (nominal) knowledge about the UAV inertia matrix $\boldsymbol{I}_b$ and mass m. $\boldsymbol{\eta}_b$ and $\dot{\boldsymbol{\eta}}_b$ can be obtained by the on-board IMU sensor, while $\dot{\boldsymbol{p}}_b$ can be estimated by employing vision and/or GPS data in outdoor scenarios, while an external visual tracking system can be employed in indoor tasks. The total thrust u and the input torque $\boldsymbol{\tau}_b^b$ are given by the controller (see Section IV).

It is worth noticing that no inversion of the inertia matrix $\boldsymbol{M}(\boldsymbol{\eta}_b)$ is required, and also no knowledge of the absolute position $\boldsymbol{p}_b$ of the UAV is needed. The dynamic parameters of the system might also not be known exactly a-priori, since it will turn out to be as the appearance of external generalized forces due to unmodeled effects. Moreover, notice that, with respect to [17], second-order transfer functions have been considered. In this way, it is possible to better weaken the effects of high-frequencies noise, specially introduced by the IMU sensor and the estimation of $\dot{\boldsymbol{p}}_b$. Finally, notice that with small modifications to (11), it is possible to obtain transfer functions in (9) of the desired order.

From (12) it is possible to recognize that the estimator is able to perfectly reconstruct external disturbances, while the reconstruction of time-varying external disturbances depends on the chosen natural frequency and damping factor in (10).

IV. VToL UAV Impedance Control

Compensating the dynamics (5b) and introducing a new virtual input torque, defined by the (3×1) vector $\bar{\boldsymbol{\tau}}$, yields

$$\boldsymbol{\tau}_b^b = \boldsymbol{I}_b\boldsymbol{Q}(\boldsymbol{\eta}_b)\bar{\boldsymbol{\tau}} + \boldsymbol{Q}(\boldsymbol{\eta}_b)^{-\mathrm{T}}\left(\boldsymbol{C}(\boldsymbol{\eta}_b,\dot{\boldsymbol{\eta}}_b)\dot{\boldsymbol{\eta}}_b - \widehat{\boldsymbol{\tau}}_{ext}\right). \tag{14}$$

By substituting (14) in (5b) it is possible to achieve

$$\ddot{\boldsymbol{\eta}}_b = \bar{\boldsymbol{\tau}} + \boldsymbol{M}(\boldsymbol{\eta}_b)^{-1}\widetilde{\boldsymbol{\tau}}, \tag{15}$$

where $\widetilde{\boldsymbol{\tau}} = \boldsymbol{\tau}_{ext} - \widehat{\boldsymbol{\tau}}_{ext}$.

Because of the under-actuation of the system, since it could be shown that $\boldsymbol{p}_b$ and ψ are flat outputs for the system (5) [22], a common way to design the control is to consider as references the desired position trajectory of the VToL UAV, described by the (3×1) vectors $\boldsymbol{p}_d$, $\dot{\boldsymbol{p}}_d$ and $\ddot{\boldsymbol{p}}_d$, and the desired yaw angle trajectory, described by ψ_d, $\dot{\psi}_d$ and $\ddot{\psi}_d$.

A new virtual input can be defined by the (3×1) vector $\boldsymbol{\mu}$ as follows

$$\boldsymbol{\mu} = \begin{bmatrix}\mu_1 & \mu_2 & \mu_3\end{bmatrix}^{\mathrm{T}} = -\frac{u}{m}\boldsymbol{R}_b(\boldsymbol{\eta}_d)\boldsymbol{e}_3 + \boldsymbol{g} + \frac{1}{m}\widehat{\boldsymbol{f}}_{ext}, \tag{16}$$

representing the desired acceleration vector with respect to Σ_i, in which the magnitude is the total thrust u produced by the propellers, while the orientation is given by the desired UAV attitude. $\boldsymbol{\eta}_d = \begin{bmatrix}\phi_d & \theta_d & \psi_d\end{bmatrix}^{\mathrm{T}}$ is the (3×1) vector of the UAV desired attitude.

Let $\boldsymbol{e}_p = \boldsymbol{p}_b - \boldsymbol{p}_d$, $\dot{\boldsymbol{e}}_p = \dot{\boldsymbol{p}}_b - \dot{\boldsymbol{p}}_d$, $\ddot{\boldsymbol{e}}_p = \ddot{\boldsymbol{p}}_b - \ddot{\boldsymbol{p}}_d$, $\boldsymbol{e}_\eta = \boldsymbol{\eta}_b - \boldsymbol{\eta}_d$, $\dot{\boldsymbol{e}}_\eta = \dot{\boldsymbol{\eta}}_b - \dot{\boldsymbol{\eta}}_d$ and $\ddot{\boldsymbol{e}}_\eta = \ddot{\boldsymbol{\eta}}_b - \ddot{\boldsymbol{\eta}}_d$ be the (3×1) tracking errors, and let $\widetilde{\boldsymbol{f}} = \boldsymbol{f}_{ext} - \widehat{\boldsymbol{f}}_{ext}$ be the estimated external forces error. Replacing both $\boldsymbol{\eta}_b = \boldsymbol{\eta}_d + \boldsymbol{e}_\eta$ and $\boldsymbol{f}_{ext} = \widehat{\boldsymbol{f}}_{ext} + \widetilde{\boldsymbol{f}}$ in (5a) and taking into account some trigonometric relations yields

$$\ddot{\boldsymbol{p}}_b = \boldsymbol{\mu} + \frac{u}{m}\boldsymbol{\delta}(\boldsymbol{\eta}_d,\boldsymbol{e}_\eta) + \frac{1}{m}\widetilde{\boldsymbol{f}}, \tag{17}$$

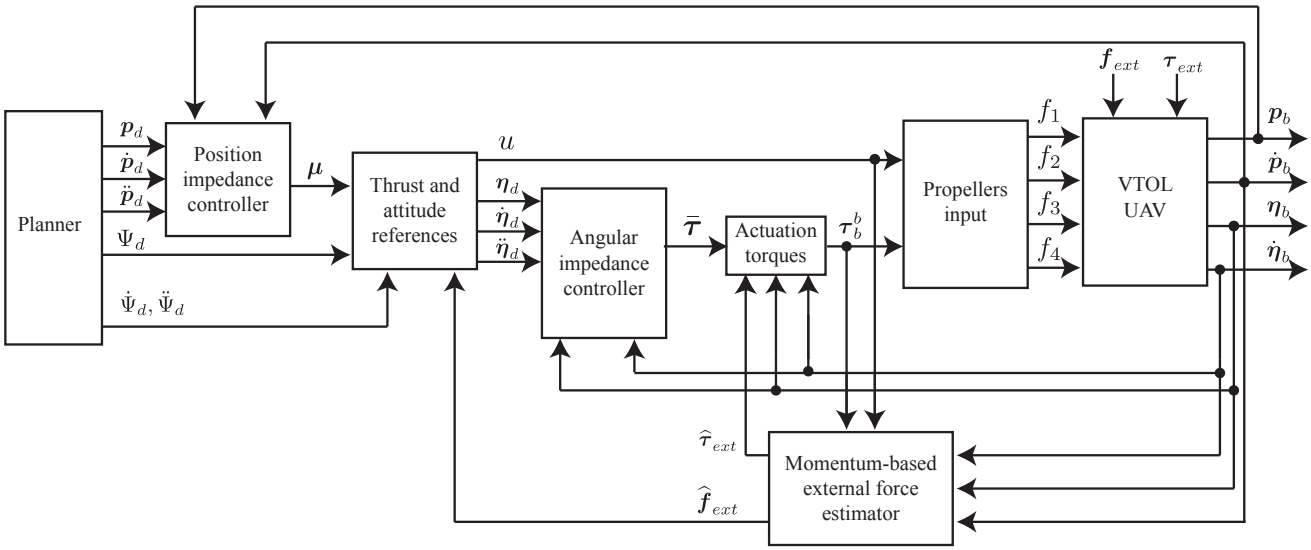

Fig. 2. Block scheme of the proposed architecture.

where $\boldsymbol{\delta}(\boldsymbol{\eta}_d, \boldsymbol{e}_\eta)$ is a (3×1) interconnection vector depending on the desired UAV attitude and the tracking error $\boldsymbol{e}_\eta$. The detailed expression for $\boldsymbol{\delta}(\boldsymbol{\eta}_d, \boldsymbol{e}_\eta)$ can be found in [13].

Hence, in order to achieve the desired closed-loop impedance behaviour, the virtual control inputs $\boldsymbol{\mu}$ and $\bar{\boldsymbol{\tau}}$ can be chosen as follows

$$\boldsymbol{\mu} = \ddot{\boldsymbol{p}}_d - \frac{1}{m}\left(\boldsymbol{D}_p\dot{\boldsymbol{e}}_p + \boldsymbol{K}_p\boldsymbol{e}_p\right), \tag{18a}$$

$$\bar{\boldsymbol{\tau}} = \ddot{\boldsymbol{\eta}}_d - \boldsymbol{M}^{-1}\left(\left(\boldsymbol{D}_o + \boldsymbol{C}(\boldsymbol{\eta}_b, \dot{\boldsymbol{\eta}}_b)\right)\dot{\boldsymbol{e}}_\eta + \boldsymbol{K}_o\boldsymbol{e}_\eta\right), \tag{18b}$$

where $\boldsymbol{D}_i$ and $\boldsymbol{K}_i$, with $i = \{p, o\}$, are (3×3) positive definite gain matrices. Therefeore, folding (18a) and (18b) into (15) and (17), respectively, yields the following closed-loop equations

$$m\ddot{\boldsymbol{e}}_p + \boldsymbol{D}_p\dot{\boldsymbol{e}}_p + \boldsymbol{K}_p\boldsymbol{e}_p = u\boldsymbol{\delta}(\boldsymbol{\eta}_d, \boldsymbol{e}_\eta) + \widetilde{\boldsymbol{f}}, \tag{19a}$$

$$\boldsymbol{M}(\boldsymbol{\eta}_b)\ddot{\boldsymbol{e}}_\eta + \left(\boldsymbol{D}_o + \boldsymbol{C}(\boldsymbol{\eta}_b, \dot{\boldsymbol{\eta}}_b)\right)\dot{\boldsymbol{e}}_\eta + \boldsymbol{K}_o\boldsymbol{e}_\eta = \widetilde{\boldsymbol{\tau}}. \tag{19b}$$

The right-side term in (19a) acts like an external force on the first sub-system and depends on both the UAV attitude error and the estimated external forces error. The right-side term in (19b) is the residual of the estimated external moments and acts as a disturbance on the second subsystem. Thus, the expressions in (19) establish a relationship between the residuals of the estimation of external disturbances and the tracking errors. This impedance is characterized by the considered mass m and inertia $\boldsymbol{M}(\boldsymbol{\eta}_b)$ of the VToL UAV, the damping matrices $\boldsymbol{D}_i$ and the stiffness matrices $\boldsymbol{K}_i$, with $i = \{p, o\}$, which can be used to specify the dynamic behaviour along the linear and angular directions of Σ_i. Notice that the damping matrix $\boldsymbol{D}_o$ only partially contributes to the total damping of the mechanical impedance.

The gains of (19) are chosen on the basis of the desired impedance behaviour for the closed-loop system. For example, a high stiffness will be chosen for free-flight trajectory-tracking tasks, while a small one should be suitable for interaction tasks. On the other hand, a high damping is always required to a UAV to avoid overshooting at the target position. Furthermore, since (19) represents a mechanical system, this is typically able to resist external disturbances having frequencies comparable with its bandwidth. Hence, the tuning of (12) can be simply made by choosing a bandwidth larger enough than that of (19), e.g. the twice.

To summarize, after computing the position tracking errors $\boldsymbol{e}_p$ and $\dot{\boldsymbol{e}}_p$, by knowing the feed-forward acceleration $\ddot{\boldsymbol{p}}_d$, the virtual control input $\boldsymbol{\mu}$ can be computed as in (18a). The desired total thrust u and the reference pitch and roll can be obtained by inverting (16) as follows

$$u = m\sqrt{\bar{\mu}_1^2 + \bar{\mu}_2^2 + (\bar{\mu}_3 + g)^2}, \tag{20a}$$

$$\phi_d = \sin^{-1}\left(m\frac{\bar{\mu}_1\sin\psi_d - \bar{\mu}_2\cos\psi_d}{u}\right), \tag{20b}$$

$$\theta_d = \tan^{-1}\left(\frac{\bar{\mu}_1\cos\psi_d + \bar{\mu}_2\sin\psi_d}{\bar{\mu}_3 + g}\right), \tag{20c}$$

where $\bar{\boldsymbol{\mu}} = \begin{bmatrix}\bar{\mu}_1 & \bar{\mu}_2 & \bar{\mu}_3\end{bmatrix}^{\mathrm{T}} = \boldsymbol{\mu} - (1/m)\widehat{\boldsymbol{f}}_{ext}$, with $\widehat{\boldsymbol{f}}_{ext}$ given by (11), while the desired yaw ψ_d is given by the planner. A second-order low-pass digital filter should be employed to reduce noise and compute both first and second derivative of $\boldsymbol{\eta}_d$, so as to get $\dot{\boldsymbol{\eta}}_d$ and $\ddot{\boldsymbol{\eta}}_d$, and hence compute in turn the attitude tracking errors $\boldsymbol{e}_\eta$ and $\dot{\boldsymbol{e}}_\eta$. The virtual control input $\bar{\boldsymbol{\tau}}$ can be obtained as in (18b), while the actuation torques vector is retrieved from (14) in which $\widehat{\boldsymbol{\tau}}_{ext}$ is given by (11). Having at disposition both the thrust u and the actuation torques $\boldsymbol{\tau}_b^b$, the propellers forces f_i, with $i = 1, \ldots, 4$, can be computed by inverting (4). The block scheme of the proposed architecture is depicted in Fig. 2.

V. Sketch of the Stability Proof

For brevity, only a sketch of the proof is here reported to prove the stability of the whole control scheme, made up of the momentum-based external generalized forces estimator and the position/angular impedance controllers.

In case of a perfect compensation of both the external forces and moments, i.e., $\widetilde{\boldsymbol{f}} = \widetilde{\boldsymbol{\tau}} = \mathbf{0}$, then $\boldsymbol{e}_p = \dot{\boldsymbol{e}}_p = \boldsymbol{e}_\eta = \dot{\boldsymbol{e}}_\eta = \mathbf{0}$ is a global asymptotically stable equilibrium point for the system (19) as shown in [13].

Otherwise, the stability proof has to take in account non-vanishing perturbations. This could be done by considering the stability theory of both perturbed and interconnected systems [23]. The rough idea behind these theories is that if an exponentially stable system is perturbed by a nonvanishing, but bounded, external disturbance, then the state variables of the system will remain bounded during time. Some results could be also provided for asymptotically stable systems.

First of all, in the presented case, the boundedness of the solutions of the momentum-based estimator has to be shown. Since it is possible to assume that the real external disturbances are always limited, the perturbation term on the right-side of (12) is bounded. Then the boundedness of $\widehat{\boldsymbol{f}}_{ext}(t)$ and $\widehat{\boldsymbol{\tau}}_{ext}(t)$ can be proved [23]. Now, a two-steps procedure is adopted. First, the stability of (19b) is verified thanks to the perturbation theory [23] and to the boundedness of $\widehat{\boldsymbol{\tau}}_{ext}(t)$. However, this is the toughest part of the proof since (19b) is a time-varying system because of the presence of the inertia matrix depending on the actual attitude of the VToL UAV [24]. Then, the stability of (19a) is verified considering the interconnection with the angular closed-loop equation as done in [13]. The boundedness of $\widehat{\boldsymbol{f}}_{ext}(t)$ is taken into account in this latter part, as well. As a result, the boundedness of solutions in (19), i.e., marginal stability, can be guaranteed since the right-side terms in (19) are bounded. Asymptotically stability can be obtained only in the unconstrained directions [20].

VI. Experimental Results

A. Set-up and Technical Details

The experiments have been performed in the PRISMA Arena which is equipped with an OptiTrack motion-capture system. The employed quadrotor is an ASCTECH PELICAN. The controller is implemented onboard (at 100Hz) on an ATOM CPU with UBUNTU OS and a patched RTAI real-time kenerel. The ground station is an external PC with UBUNTU OS and it is in charge of the WiFi communication between the OptiTrack system and the vehicle, as well as for the operator telemetry and human interfacing.

The estimated mass and inertia matrix of the vehicle are 1.2 Kg and $\boldsymbol{I}_b = \mathrm{diag}(3.4, 3.4, 4.7)10^{-3}$ Kgm^2, respectively.

The natural frequency and the damping factor for the closed-loop linear impedance have been chosen as 4 rad/s and 1, respectively. Hence, the gains in (18a) have been tuned to $\boldsymbol{K}_p = 16\boldsymbol{I}_3$ and $\boldsymbol{D}_p = 12\boldsymbol{I}_3$, following the relations in (13). Since the rotational part is faster than the linear one, the natural frequency for the closed-loop rotational impedance (18b) has been chosen twice the linear one. The damping factor is again tuned to 1. The procedure described in [24] has been adopted to tune $\boldsymbol{D}_o$. Consequently, the desired natural frequency and damping factor for the estimator have been chosen as 10 rad/s and 1, respectively, for all the components in (10).

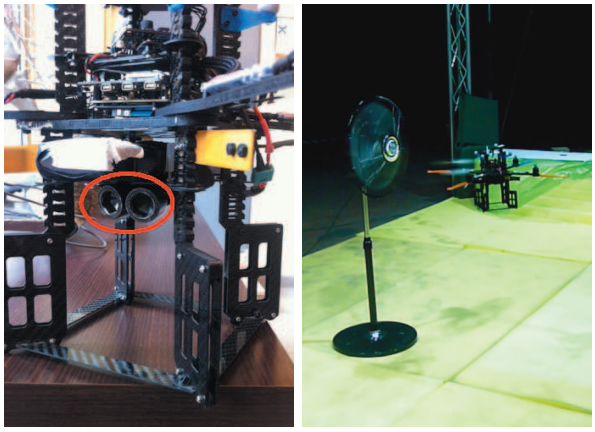

Fig. 3. On the left, the additional load placed below the battery compartment is highlighted by a red ellipse. On the right, the quadrotor in front of the fan.

B. Case Studies

In all the considered case studies, the performance of the proposed control design (from now on called PD+C[1] for brevity) is compared to classical PD and PID approaches. In detail, the PD control has been implemented without considering the compensation of the estimated external generalized forces, i.e., $\widehat{\boldsymbol{\tau}}_{ext}$ is not present in (14) and $\bar{\boldsymbol{\mu}} = \boldsymbol{\mu}$ in (20). The control gains are kept as in the PD+C case. On the other hand, the PID control has been implemented as the PD one with the addition of an integral action in (18). The gain of this integral term has been set to $0.5\boldsymbol{I}_3$.

Three case studies are considered in the following. Other case studies are presented in the multimedia attachment, showing the performance of the proposed controller in several different situations, e.g., interaction with an operator, pendulum attached at the bottom of the vehicle, and so on.

1) Case study A: In this case study, the quadrotor performs a hovering task at an altitude of 1 m with respect to the ground. An additional load of about 0.110 Kg (about 8% of the UAV mass m) has been placed in the battery compartment of the vehicle (see Fig. 3) but not considered in the control.

The comparison between the PD+C, PD and PID controllers is depicted in Fig. 4. The landing part is omitted. From Fig. 4(a) it is possible to recognize that the norm of the position error for the PD+C controller is lower than the one obtained with the other implemented controllers. In particular, the PD is not able to recover the error due to the additional load placed on the quadrotor. The integral action in the PID recovers this information with a speed depending on the chosen gain, which in any case should be accurately tuned so as not to compromise the stability of the vehicle. Moreover, Fig. 4(b) shows how the oscillations around the fixed hovering point are reduced by using the proposed PD+C controller. The quadrotor control inputs are depicted in Fig. 4(d). The lines do not start from zero since

[1]PD+C stands for PD control plus compensation of the estimated external generalized forces

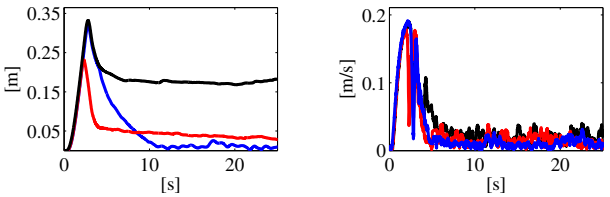

(a) Position error norm. (b) Linear velocity error norm.

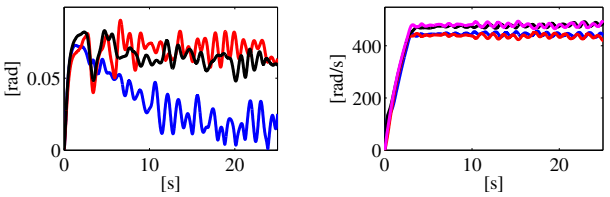

(c) Attitude error norm. (d) Propellers angular velocity

Fig. 4. Case study A. Hovering with additional load. Performance evaluation. From subfigure (a) to (c) the legend is: blue, PD+C; red, PID; black, PD. Subfigure (d) shows the angular velocity of the propellers 1,2,3 and 4 (blue, red, black, magenta) in the PD+C case.

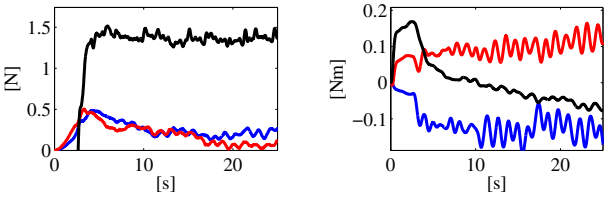

(a) External forces estimation (b) External moments estimation

Fig. 5. Case study A. Hovering with additional load. Estimated external forces and moments along (around) the axes x, y and z (blue, red, black) employed in the PD+C case.

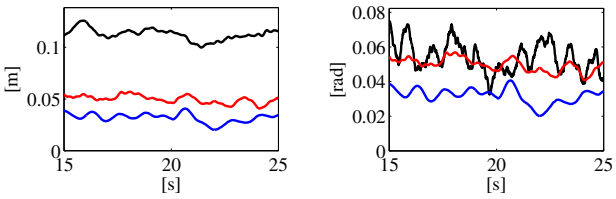

(a) Position error norm. (b) Attitude error norm.

Fig. 6. Case study B. Hovering, in front of a fan, with additional load. Performance evaluation. The legend is: blue, PD+C; red, PID; black, PD.

the propellers are rotating at a slow velocity before the take-off command is provided to the quadrotor. The estimated external forces and moments are displayed in Fig. 5. The uncertainty about the knowledge of the inertia matrix $\boldsymbol{I}_b$ is highlighted in the values different from zero in Fig. 5(b). The presence of the additional load on the UAV is evidenced in the z component of the estimated external force in Fig. 5(a).

2) Case study B: This case study is similar to the previous one with the addition of a fan producing wind at a distance of 0.15 m from the quadrotor (see Fig. 3).

In Fig. 6 the comparison between the PD+C, PD and PID controllers is depicted. Only the hovering part is considered in the related time histories. In Fig. 6(a) it is possible to

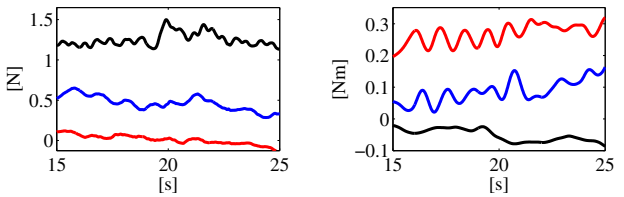

(a) External forces estimation (b) External moments estimation

Fig. 7. Case study B. Hovering, in front of a fan, with additional load. Estimated external forces and moments along (around) the axes x, y and z (blue, red, black) employed in the PD+C case.

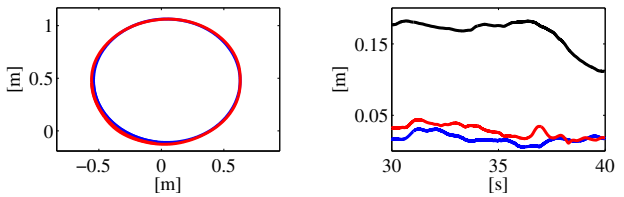

(a) Circle (b) Position error norm.

Fig. 8. Case study C. Circular trajectory with additional load. Performance evaluation. In subfigure (a) the circle in blue is the reference, the circle in red is the one executed under the PD+C control. The legend for subfigure (b) is: blue, PD+C; red, PID; black, PD.

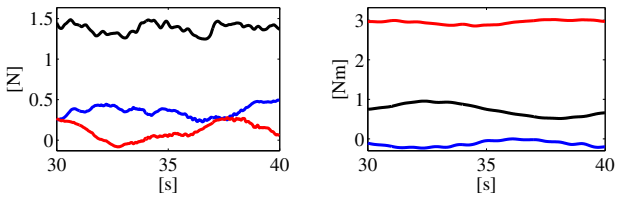

(a) External forces estimation (b) External moments estimation

Fig. 9. Case study C. Circular trajectory with additional load. Estimated external forces and moments along (around) the axes x, y and z (blue, red, black) employed in the PD+C case.

recognize that the norm of the position error for the PD+C controller is lower than the one obtained with the other implemented controllers. In particular, due to the persistent external disturbance, the error can be zeroed only along the unconstrained directions, resulting in an almost constant position error norm during time. The estimated external forces and moments are depicted in Fig. 7. It is still possible to notice the estimation of the force due to the additional load. Moreover, with respect to Fig. 5(a), it is possible to notice a higher value of the estimated force in Fig. 7(a), especially along the x direction due to the presence of the wind force which is hence properly reconstructed.

3) Case study C: In this case study, the quadrotor tracks a circle of a given radius with a constant speed of 0.5 m/s. The circle is planned in the x, y plane at a constant altitude from the ground and it is executed twice. Like the two previous case studies, an additional load of about 0.110 Kg has been placed in the battery compartment of the vehicle, but not considered in the control. First, the quadrotor performs the take-off reaching the hovering condition at 1 m from the ground. Then, after a fixed amount of time, the command

to perform the tracking of the circle is given to the vehicle. Once the trajectory has been completed, the quadrotor lands. In the time histories of Fig. 8 only the circular trajectory is displayed, neglecting the other phases.

In Fig. 8(a), it is possible to appreciate the tracking performance (and the repeatability of the trajectory) of the PD+C controller with respect to the planned circle in the x, y plane. The comparison between the PD+C, PD and PID controllers is provided in Fig. 8(b). Again, the norm of the position error for the PD+C controller is lower than the one obtained with the other implemented controllers. The estimated external forces and moments are depicted in Fig. 9. Due to the presence of the unbalanced added weight during the execution of the circular trajectory, significant moments are also estimated, as shown in Fig. 9(b).

VII. Conclusion and Future Work

In this paper, a momentum-based estimator of external generalized forces has been proposed to control a VToL UAV together with a suitably modified hierarchical architecture, shaping the closed-loop equations as mechanical impedances programmable through the control gains. This arrangement allows the VToL UAV to perform hovering and tracking tasks without a precise knowledge of the vehicle dynamics and in presence of external disturbances. Experimental results have been presented to prove the performance of the proposed control design with respect to other classical controllers employed in aerial robotics.

Future work will be focused on problems related to outdoor scenarios. In particular, the effects of introducing an estimated linear velocity, rather than using the one provided by high-frequency external visual tracker, will be examined. A detailed stability proof of the whole framework will be provided in a future extended version of this work, taking into account the problems related to the interconnection between the external generalized forces estimator and the VToL UAV hierarchical controller.

References

[1] V. Lippiello and B. Siciliano, "Wall inspection control of a VTOL unmanned aerial vehicle based on a stereo optical flow," in *2012 IEEE/RSJ International Conference on Intelligent Robots ans Systems*, (Vilamoura, P), pp. 4296–4302, 2012.

[2] L. Marconi, L. Basile, G. Caprari, R. Carloni, P. Chiacchio, C. Huerzeler, V. Lippiello, R. Naldi, N. Janosch, B. Siciliano, S. Stramigioli, and E. Zwicker, "Aerial service robotics: The AIRobots perspective," in *2nd International Conference on Applied Robotics for the Power Industry*, (Zurich, CH), 2012.

[3] P. Pounds, D. Bersak, and A. Dollar, "Grasping from the air: Hovering capture and load stability," in *2011 IEEE International Conference on Robotics and Automation*, (Shanghai, CN), pp. 2491–2498, 2011.

[4] G. Arleo, F. Caccavale, G. Muscio, and F. Pierri, "Control of quadrotor aerial vehicles equipped with a robotic arm," in *21st Mediterranean Conference on Control and Automation*, (Crete, GR), 2013.

[5] F. Forte, R. Naldi, A. Macchelli, and L. Marconi, "Impedance control of an aerial manipulator," in *Proceedings of 2012 American Control Conference*, (Montreal, CDN), pp. 3839–3844, 2012.

[6] V. Lippiello and F. Ruggiero, "Exploiting redundancy in Cartesian impedance control of UAVs equipped with a robotic arm," in *2012 IEEE/RSJ International Conference on Intelligent Robots ans Systems*, (Vilamoura, P), pp. 3768–3773, 2012.

[7] V. Lippiello and F. Ruggiero, "Cartesian impedance control of a UAV with a robotic arm," in *10th International IFAC Symposium on Robot Control*, (Dubrovnik, HR), pp. 704–709, 2012.

[8] T. Madani and A. Benallegue, "Sliding mode observer and backstepping control for a quadrotor unmanned aerial vehicles," in *Proceedings of the 2007 American Control Conference*, (New York City, NY), pp. 5887–5892, 2007.

[9] V. Lippiello, G. Loianno, and B. Siciliano, "MAV indoor navigation based on a closed-form solution for absolute scale velocity estimation using optical flow and inertial data," in *50th IEEE Conference on Decision Control and European Control Conference*, (Orlando, FL), pp. 3566–3571, 2011.

[10] R. Carloni, V. Lippiello, M. D'Auria, M. Fumagalli, A. Mersha, S. Stramigioli, and B. Siciliano, "Robot vision: Obstacle-avoidance techniques for unmanned aerial vehicles," *IEEE Robotics & Automation Magazine*, vol. 20, no. 4, pp. 22–31, 2013.

[11] R. Mahony, S. Stramigioli, and J. Trumpf, "Vision based control of aerial robotic vehicles using the port Hamiltonian framework," in *50th IEEE Conference on Decision Control and European Control Conference*, (Orlando, FL), pp. 3526–3532, 2011.

[12] R. Mahony and T. Hamel, "Robust trajectory tracking for a scale model autonomous helicopter," *International Journal of Robust and Nonlinear Control*, vol. 14, no. 12, pp. 1035–1059, 2004.

[13] K. Nonami, F. Kendoul, S. Suzuki, and W. Wang, *Autonomous Flying Robots. Unmanned Aerial Vehicles and Micro Aerial Vehicles*. Berlin Heidelberg, D: Springer-Verlag, 2010.

[14] A. Roberts and A. Tayebi, "Adaptive position tracking of VTOL UAVs," *IEEE Transactions on Robotics*, vol. 27, no. 1, pp. 129–142, 2011.

[15] I. Palunko, P. Cruz, and R. Fierro, "Agile load transportation. Safe and efficient load manipulation with aerial robots," *Robotics & Automation Magazine*, vol. 19, no. 3, pp. 69–79, 2012.

[16] G. Antonelli, F. Arrichiello, S. Chiaverini, and P. Robuffo Giordano, "Adaptive trajectory tracking for quadrotor MAVs in presence of parameter uncertainties and external disturbances," in *Proceedings 2013 IEEE/ASME International Conference on Advanced Intelligent Mechatronic*, (Wollongong, AU), pp. 1337–1342, 2013.

[17] A. De Luca, A. Albu-Schaffer, S. Haddadin, and G. Hirzinger, "Collision detection and safe reaction with the DLR-III lightweight manipulator arm," in *IEEE/RSJ International Conference on Intelligent Robots ans Systems*, (Beijing, C), pp. 1623–1630, 2006.

[18] H. Sadeghian, L. Villani, M. Keshmiri, and B. Siciliano, "Task space control of robot manipulators with null space compliance," *IEEE Transactions on Robotics*, 2013 (in press, available online).

[19] G. Antonelli, "On the use of adaptive/integral actions for 6-degrees-offreedom control of autonomous underwater vehicles," *IEEE Journal of Oceanic Engineering*, vol. 32, no. 2, pp. 300–312, 2007.

[20] B. Siciliano, L. Sciavicco, L. Villani, and G. Oriolo, *Robotics: Modelling, Planning and Control*. London, UK: Springer, 2008.

[21] T. Madani and A. Benallegue, "Backstepping control for a quadrotor helicopter," in *IEEE/RSJ International Conference on Intelligent Robots ans Systems*, (Beijing, C), pp. 3255–3260, 2006.

[22] P. Fliess, J. Levine, and P. Rouchon, "Flatness and defect of nonlinear systems: Introductory theory and examples," *International Journal of Control*, vol. 61, no. 6, pp. 1327–1361, 1995.

[23] H. Khalil, *Nonlinear systems*. Upper Saddle River, NJ: Prentice Hall, 2002.

[24] C. Ott, *Cartesian Impedance Control of Redundant and Flexible-Joint Robots*, vol. 49 of *Springer Tracts in Advanced Robotics*. Berlin Heidelberg, D: Springer-Verlag, 2008.